

OPEN ACCESS

DC Sputtered Ultralow Loading Gold Nanofilm Electrodes for Detection of As (III) in Water

To cite this article: Tybur Q. Casuse et al 2022 ECS Sens. Plus 1 014602

View the <u>article online</u> for updates and enhancements.





DC Sputtered Ultralow Loading Gold Nanofilm Electrodes for Detection of As (III) in Water

Tybur Q. Casuse,^{1,*} Angelica Benavidez,² John B. Plumley,² Lok-kun Tsui,^{2,*} Abdul-Mehdi Ali,³ José M. Cerrato,¹ and Fernando H. Garzon^{2,*,z}

This study investigates the use of DC sputtering, physical vapor deposition as a facile method for creating ultralow loading, Au/C electrodes for use in the detection of As (III) in water. The sputtered nanofilm electrodes on carbon papers, substantially reduces the amount of Au consumed per electrode, $<10~\mu g~cm^{-2}$, compared to use of wire, foil, or screen-printed electrodes. Linear stripping voltammetry (LSV) was chosen for analytical simplicity and ease of automation. Electrodes using Au nanoparticles supported on Vulcan XC 72 R carbon were also investigated but were not viable for LSV analysis due to capacitive current charging of the high surface area carbon. The DC sputtered, Au nanofilm electrodes were used to create calibration curves for concentrations of As (III) between 5 and 50 $\mu g~l^{-1}$ and the standard addition method was used in a surface water sample with 5.5 $\mu g~l^{-1}$ total As. Peak areas plotted against concentration displayed strong linear correlation with meaningful detection below the USEPA maximum contaminant level (MCL) of $10~\mu g~l^{-1}$. To our knowledge, this is the first study which utilizes the facile and mass manufacturable DC sputtering method to produce As (III) sensing electrodes. The results of this study have implications for the development of single use, low-cost nanofilm electrodes for field As (III) electroanalysis.

© 2022 The Author(s). Published on behalf of The Electrochemical Society by IOP Publishing Limited. This is an open access article distributed under the terms of the Creative Commons Attribution 4.0 License (CC BY, http://creativecommons.org/licenses/by/4.0/), which permits unrestricted reuse of the work in any medium, provided the original work is properly cited. [DOI: 10.1149/2754-2726/ac6d67]

Manuscript submitted March 6, 2022; revised manuscript received May 4, 2022. Published May 19, 2022.

Supplementary material for this article is available online

Unsafe concentrations of arsenic (As) in drinking water are a global health hazard afflicting many areas of the world such as Argentina, United States, Bangladesh and Vietnam. 1,2 Concentrations as low as $10 \,\mu g \, l^{-1}$ in daily drinking water have been identified to cause chronic detrimental health effects according to The United States Environmental Protection Agency (USEPA) and World Health Organization (WHO).^{3,4} The solubilization of As (III) is commonly performed through microbial respiration in anoxic soils and is dependent on a multitude of variables including temperature and presence of elements such as iron, sulfide, manganese and carbon. 5-10 Many naturally occurring minerals contain As which can be mobilized into ground or surface waters by either reducing or oxidizing conditions to form oxyanions primarily containing arsenite, As (III), and arsenate, As (V), respectively. 11 Arsenic can be found in valence states of -3, -1, 0, +3 and +5, however +3 and +5 are the most common forms in natural waters and present the most concern for toxicity from ingestion. The mobilization of As (III) in anoxic soils can lead to unsafe concentrations in aquifers which may unknowingly be used as a potable water source.

Several methods for quantitative analysis of μ g l⁻¹ As concentrations are available both in the laboratory and in the field. ^{12,13} laboratory methods include atomic absorption spectroscopy, inductively coupled plasma mass spectrometry and atomic fluorescence spectroscopy. High cost per sample and transport to a capable facility are limitations when conducting studies that require many sample sites, remote locations, or time dependence. Currently, in field measurements can be done by colorimetric techniques and electrochemical sensors. ^{14,15} For example, Metrohm produces a three-electrode sensor which uses a Au wire working electrode (WE) with a 0.3μ g l⁻¹ limit of detection (LOD) and results are obtained in around 2 min. ¹⁶ Creating electroanalysis calibration curves in field samples helps to investigate novel electrodes for their in situ capabilities and identify competing ion effects. ^{17,18} Electroanalysis has many advantages for in situ applications

including lightweight materials, low detection limits, and rapid on-

site results, which is especially valuable in well bore installation

lume ratio compared to macroelectrodes, such as wires. Gold (Au),

platinum (Pt) and silver (Ag) are the most commonly studied electrode materials due to their catalytic activity, stability and wide potential range for analysis. ^{19,20} Gold is the most ideal of

these options due to its high overpotential for hydrogen evolution

and stability within the potentials at which As (III) is reduced and oxidized between the zero and trivalent state. ²¹ Gold nanoparticles

and films have been synthesized in a variety of methods using

chemical deposition or electrodeposition onto conductive substrates,

typically electrically conductive carbons. 17,22-31 The use of nanos-

tructures such as nanoparticles and nanofilms increases the useable

surface area per mass of Au for the electrode, leading to a decrease

physical vapor deposition (PVD) techniques can be used for

Thin films of Au with nanoscale thicknesses generated with

Nano-structured electrodes offer increased surface area to vo-

applications or testing in remote locations.

in precious metal consumption.

in remote and developing world locations, low-cost and high volume manufacturing of these electrodes would help to increase the availability of potentially lifesaving knowledge to vulnerable communities. Our study is aligned with recent efforts to develop facile and low-cost electrode fabrication methods beyond screen printing and Au wire electrodes, which could increase access to electrochemical detection. Therefore, this study seeks to investigate the suitability of electrodes prepared by DC sputtered to be used as an alternative to nanoparticle, screen printing, and wire electrodes.

This is the first investigation presenting the use of ultralow ($<10 \,\mu\mathrm{g}\,\mathrm{cm}^{-2}$) gold loading on carbon, formed using sputter

¹Department of Civil, Construction & Environmental Engineering, University of New Mexico, Albuquerque, New Mexico 87131, United States of America

²Center for Micro Engineered Materials, Albuquerque, New Mexico 87106, United States of America

³ Department of Earth & Planetary Sciences, University of New Mexico, Albuquerque, New Mexico 87131, United States of America

fabricating ultralow loading electrodes. Direct current (DC) or Radio Frequency (RF) sputter deposition is a particularly common manufacturing method for coatings of thin films in large production operations such as the automotive and textile industries. ^{32,33} Physical vapor deposition of Au thin films has also been used with various substrates such as TiO₂, quartz glass, and poly(methyl methacrylate) (PMMA) substrates and used for other electrochemical applications. ^{34–37} Due to a global need for detection of As (III)

^{*}Electrochemical Society Member.

^zE-mail: garzon@unm.edu

deposition, to detect As (III) in water. This method may significantly impact the development of low-cost systems that use linear stripping voltammetry for As (III) detection and could be economically accessible to under-served communities. Regional As prevalence investigations may require the analysis of hundreds to thousands of water samples. Near real-time measurements of water samples during well drilling operations are particularly valuable in selecting appropriate aquifers with low As concentrations. While in some cases, bulk Au electrodes may be cleaned and reused, practical field cleaning is problematic and time consuming. The replacement cost of single use, stripping electrodes may limit the scope of timely field investigations. Implementation of this electrode fabrication method contributes to in situ trace As detection by generating consumable electrodes that are analytically effective, ultralow Au loading, and scalable by using existing manufacturing techniques. Herein, we investigate the use of DC sputter deposition, Au nanofilms on carbon paper supports to detect below the MCL of As (III) in ultrapure water as well as a complex surface water sample which was comprehensively analyzed for species present using spectroscopic and chromatography laboratory techniques.

Experimental

Generation of Au nanofilm and nanoparticle electrodes.—We fabricated two types of Au nanostructured electrodes, one with DC sputter deposition of Au nanofilm s and another with chemical deposition of Au nanoparticles onto carbon nanoparticles then bonded onto carbon support. Both methods provide means for very low—cost synthesis of consumable electrodes for field investigations. Electrodeposition of Au nanoparticles onto conductive supports, although viable, was not explored due to the increased cost and complexity of deposition for large numbers of electrodes. For the DC sputtered electrodes, Au was deposited directly onto both sides of a 1 cm wide by 5 cm long Sigracet 29AA carbon paper. Sputter coaters manufactured by Polaron or SPI DC were used for Au deposition, voltage 1.7 kV, current 18 mA, and deposition times from 60 to 120 s. An Au lead wire was woven into the dry portion of the carbon paper, providing a robust method of electrode current collection.

The nanoparticles were synthesized using Vulcan XC 72 R (\sim 250 m² g⁻¹ surface area, 50 nm particle size) carbon supports. The XC 72R was functionalized in a 24 h reflux of 2.5% nitric acid at 93 °C. ⁴³ A ratio of 0.62 wt/wt% polyvinyl alcohol (PVA) to Au was used to create a colloidal solution. 44 Sodium borohydride (NaBH₄) was added in four times the molar concentration of Au to reduce the Au solution. The solution color changed from a transparent yellow to a deep violet color upon addition of the NaBH₄. The Au solution was then slowly dripped into a sonicating bath of the functionalized XC 72R in deionized (DI) water over approximately 15 min. The solution was sonicated in the bath for an additional hour and left to settle overnight. The solution was then centrifuged, and the supernatant was replaced with fresh DI water. The carbon with Au was mixed into the new DI water and centrifuged again. The rinsing process was repeated until the pH of the supernatant was the same as the DI water, typically four rinses. The Au on carbon was then allowed to dry at 60 °C in air and scraped into a crucible for a reduction process. The reduction was conducted in 3% H_2 balance N_2 at 320 ${}^{\circ}C$ for five hours with a ramp rate of 5° per minute from room temperature to 320° and allowed to cool to room temperature under the 3% H₂ flow. The powder was then made into an ink using 15 wt/wt% Nafion to Au/XC 72R and ethanol. The entirety of the ink was evenly painted onto both sides of a 1 x 1 cm square at the end of a 1 cm wide by 5 cm long strip of Sigracet 29 AA using a small paintbrush. Creative Materials GPC 251 electrically conductive adhesive was used to attach the carbon strip to a 1 cm wide strip of copper foil or nickel wire, which were used as a lead material. Crystal Bond 509 was used to mask the areas of the electrodes besides the Au electrode area.

An Au wire electrode was created for a comparison to a macroelectrode. Alfa Aesar 0.1 mm diameter Au wire (99.95%) was polished using an alumina slurry and wrapped around a polished nickel wire which acted as the lead and structural support of the electrode. Crystal Bond 509 was used to isolate a 3.3 cm length of the Au wire and keep the nickel wire from interacting with the electrolyte solution. A voltmeter was used to confirm conductivity between the Au and Nickle wire after Crystal bond was applied.

Solutions.—Calibration curves were created in 18 MΩ deionized (DI) water and a river water sample collected directly from the Rio Paguate River which is downstream of the Jackpile mine in Laguna, New Mexico. A previous study from our group has provided a detailed characterization of the water quality and environmental conditions of this site. For As (III) detection the solutions were acidified to 0.5 M H₂SO₄. The solution was bubbled with nitrogen and stirred using a stir bar on a moderate setting which was consistent during the deposition processes. Stirring was stopped during the stripping process. Sigma Aldrich sodium (meta)arsenite salt, NaAsO₂, was used to create a stock solution of 10^{-3} M As (III) in ultrapure water. This concentration was used to determine the amount of stock solution to add to the electrolyte to create additions of 5, 10, 25, 50 and 75 μg·l⁻¹ As (III) for LSV analysis.

Linear stripping voltammetry.—In-field electrochemical sensing typically utilizes the linear stripping voltammetry method, which is comprised of a pre-conditioning, pre-concentration and stripping periods. In the case of anodic stripping voltammetry the preconditioning period is when the electrode surface is held at a potential positive to that of the analytes oxidation to strip any remaining analyte from the surface before analysis. During the preconcentration period the electrode potential is stepped to a potential which negative to the reduction of the analyte and held for a consistent amount of time for all analysis. Finally, in the stripping step the potential is gradually swept positively until it is well beyond the peak caused by oxidation of the analyte. The potential on the Au electrodes was held at -0.1 V for 60 s to concentrate As (III) onto the electrode, a Pine Research, single junction, saturated silver chloride (Ag/AgCl) reference electrode was used as the reference electrode for all electrochemical experiments. Subsequently, the voltage was swept to 0.5 V at a rate of 10 mV s⁻¹. The standard potential for As (III) redox is expected to be near 0.051 V vs Ag/AgCl so this potential region is sufficient to observe the stripping reaction. Peak area was calculated by using the difference between the known standard addition curve and the baseline curve by aligning the two curves at the beginning and end of the oxidation peak.

Material characterization.—X-ray diffraction (XRD) analyses were conducted in a PANalytical Xpert pro instrument using Cu K α radiation operated at 40 kV and 40 mA. The data were analyzed by the MDI Jade (version 9) software package using the Whole Profile Fitting (WPF) feature. The data was taken from $2\theta = 10^{\circ}$ to 100° with a scan rate of 3° per minute. Scanning electron microscopy (SEM) analyses were conducted using a Hitachi S5200 nano SEM instrument with 10 kV and 8 mA. Transmission electron microscopy (TEM) analyses were performed with a Joel 2010F field emission gun operated at 200 kV and the images were recorded and analyzed using digital micrograph software. X-ray fluorescence (XRF) measurements were performed under vacuum with an EDAX Orbis Micro-XRF at 20 kV and 400 mA and a spot size of 1 mm in diameter. The Orbis Film builder application was utilized to compare intensity of the film to the intensity of a thick standard piece of Au to estimate mass loading of the Au film. Thermogravimetric analyses were performed using a TA instruments SDT-Q600 in air from room temperature to 800 °C at a scan rate of 5° per min.

Table I. Inductively coupled plasma (ICP) mass spectroscopy and ICP optical emission spectroscopy analysis of Laguna, NM, USA groundwater sample.

Analyte	$ICP - MS \mu \text{ g } 1^{-1}$	$ICP - OES \text{ mg } 1^{-1}$
As	5.54	_
Pb	5.19	_
U	40.38	_
Cr	3.36	_
Al	_	0.01
K	_	16.32
Ca	_	269.21
Mg	_	122.52
Na	_	391.5
Cl	_	16.9
NO_3	_	1.2
SO_4	_	2028.1
Alkalinity as CaCO	-	247

Statistical analysis.—Anova single factor tests ($\propto = 0.05$) were used in excel software to determine statistically significant differences of Au reduction max peak current potential (V) between the three Au electrodes. Plots representing three of each electrode were created and the minimum current for Au reduction at a scan rate of 50 mV s⁻¹ was used to analyze significant variation of reduction peak potentials. Anova analysis was also performed on the area $(\mu A \text{ V})$ between 5, 10 and 15 $\mu g l^{-1}$ standard additions curves and the baseline curve of the As (III) in acidified ultrapure and river water. The anova tests were used to determine statistically significant differences between the three lowest concentrations and verify the ability to detect below $10 \mu g l^{-1}$. Plots were generated using OriginPro software and the LSV data was smoothed using 5 points of window with adjacent averaging as well as vertically translated to represent the data analysis process and make the curve easier to interpret visually. Limits of detection were determined using the equation LOD = (k * Sb)/m, where k was equal to 3 for a 98.3% confidence level, Sb is the standard deviation for analysis of three blank curves, and m is the slope of the calibration curve.

River water sample analysis.—The river water sample was collected directly from the Rio Paguate Moquino River on September 21st 2020 on Laguna reservation in New Mexico, USA. The sample was not filtered or acidified at collection but was acidified to 0.5 M H₂SO₄ before LSV analysis. For Inductively Coupled Plasma (ICP) analysis the sample was filtered through a $0.45 \mu m$ membrane and acidified below pH 2 (by adding 2% HNO₃). The original pH at collection was measured to be 8.36. A PerkinElmer Optima 5300DV ICP Optical Emission Spectrometer (ICP-OES) was used to identify the major contributions of metal ions to the water matrix and analyzed Al, As, Ca, Cr, K, Mg, Na, Pb, and U. A PerkinElmer NexION 300D (Dynamic Reaction Cell) ICP Mass Spectrometer (ICP-MS) was used for trace element (As, Pb, U and Cr) analysis. Chloride, nitrate, and sulfate were measured using ion chromatography. Alkalinity was measured via acidimetric titration. The results presented in Table I of this manuscript reports only the elements which had concentrations above the limit of detection for the ICP and IC analysis.

Results and Discussion

Physical characterization of Au nanofilm and Au nanoparticles.— A nanofilm of Au was sputtered over the top of a conductive carbon paper to create the Au nanofilm electrode. The Au on carbon was analyzed by XRF and SEM. For a 60 s deposition, X-ray fluorescence analysis reported a thickness of 6.82 ± 0.42 nm with an assumption of a continuous nanofilm (Table SI (available online at stacks.iop.org/ ECSSP/1/014602/mmedia)). The nanofilm is dispersed over the top

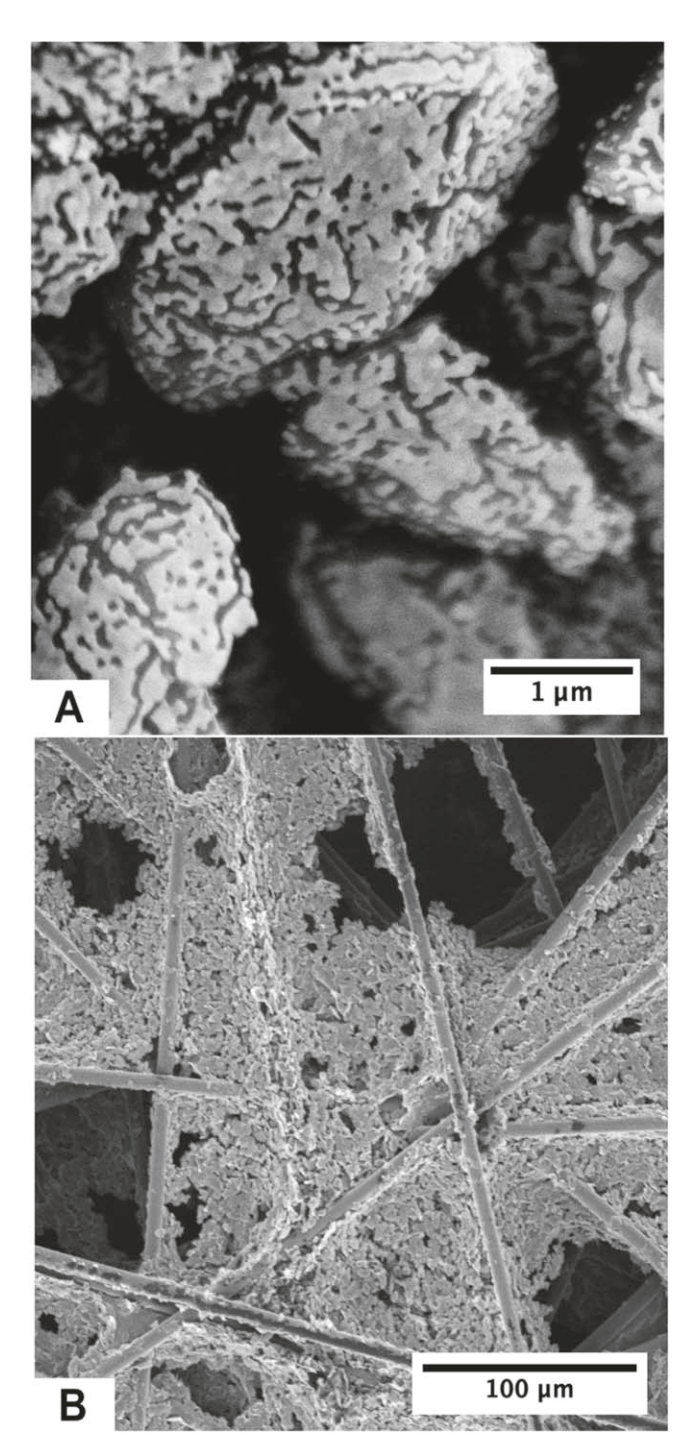


Figure 1. Gold nanofilm vapor deposited onto Sigracet 29AA. Scanning Electron Microscopy images SEM image at: (A) $10.0~\text{kV} \times 20{,}100~\text{and}$; (B) $10.0~\text{kV} \times 300$.

layer of the carbon and is not continuous, because the DC sputtering process coats the fibrous carbon with a porous film nonuniformly (Figs. 1A and 1B). Decreased Au consumption per electrode has important implications for in situ implementation in an As sensor with consumable electrodes. Over the lifetime of the electrodes many determinations of As will eventually lead to fouling of the Au surface. Electrochemical cleaning of the Au nanofilms can extend the life of the electrode, ⁴⁶ but eventually replacement will be necessary. The facile DC sputtering method can make electrode replacement less supply prohibitive and consumptive by producing large batches of low Au loading electrodes. The conditions of DC sputtering in this study did not result in a strong preferred orientation. However, by implementing

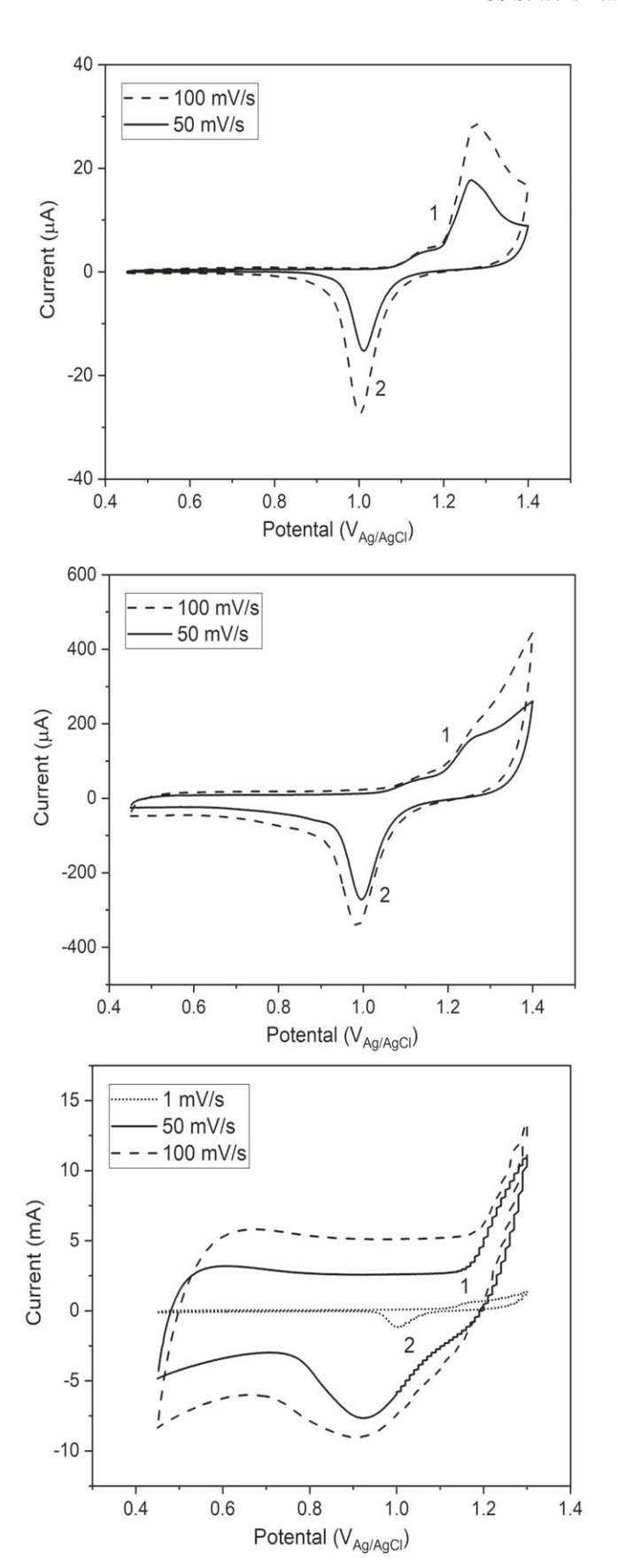


Figure 2. Cyclic voltammetry of Au surface oxidation [1] and reduction [2] in 0.5 M H_2SO_4 : (A) Au wire, geometric surface area (GSA) = 1.2 cm² [50, 100 mV s⁻¹]; (B) Au nanofilm GSA = 2 cm² [50, 100 mV s⁻¹]; (C) Au nanoparticles GSA = 460 cm² [1, 50, 100 mV s⁻¹].

annealing processes, and/or potential cycling, preferred orientation may be developed while still utilizing a low loading of Au. 34,36,47-49

The synthesis of the chemically deposited nanoparticles on XC72R carbon produced a powder that was analyzed with XRD and TEM. X-ray diffraction peaks showed that the Au nanoparticles deposited onto Vulcan XC 72R presented peaks that aligned well with International Centre for Diffraction Data (ICDD) card (PDF# 00-066-0091) peak positions for Au and gave an average crystallite size of 8 nm (Fig. S1A). The synthesis was done five separate times and resulted in average particle sizes ranging from 3 to 8 nm in size (Table SII). The crystallite size was determined using the full width and half max of the XRD peaks in the MDI Jade (version 9) software, and the Scherrer equation. Figure S1B presents a highresolution TEM image representative of the sample and corroborates the nanoparticle size determined by XRD. The image also shows that the Au particles are embedded into the carbon substrate, which will provide a physical path for electrical conductivity from the particle to the substrate. However, a portion of the surface of the particle is still exposed to the electrolyte solution, which allows the Au to interact with the ions in solution. Dark field TEM imaging showed that the Au nanoparticles were well-dispersed on the carbon support (Fig. S1C). Active sites for electrochemical reactions with redox active ions in the solution are increased by the presence of many small particles dispersed across the surface of the carbon. Using thermogravimetric analysis, the Au/C ratio was found to be 17.8 wt/wt% (Fig. S2). The geometric surface areas of Au nanoparticles and XC 72R were estimated to be near 460 cm² and 13,700 cm², respectively, by using the diameters of the particles. This Au nanoparticle electrode generation process was not as scalable as the vapor phase Au nanofilm generation process. The Au to carbon surface area ratio was much lower for the nanoparticles than the nanofilm electrode. Additional cyclic voltammetry analysis was conducted with the Au nanofilm and Au nanoparticles to evaluate their electrochemical response.

Cyclic voltammetry of Au nanofilm and Au nanoparticle electrodes.—The Au nanofilm and Au nanoparticle electrodes were compared to Au wire electrodes using cyclic voltammetry (CV) and evaluated for their ability to perform LSV. The nanofilm electrode resulted in a CV shape similar to the Au wire with an increased background current at 50 and 100 mV s⁻¹. The nanoparticle electrode presented capacitive masking of faradaic peaks at typical scan rates for LSV and showed a similar CV shape to the Au wire only at very low scan rates (Fig. 2).

The Au nanofilm was determined to be viable for LSV, because the capacitance and therefore the background current was low and allowed for consistent analysis in a large range of scan rates. Scan rates of 50 mV s⁻¹ and 100 mV s⁻¹ with the Au nanofilm produced peaks to background ratios similar to the Au wire with a manageable amount of capacitive current in the response (Figs. 2A, 2B). The reduction peak potential for the Au nanofilm was not significantly different (p = 0.25) from the Au wire (Fig. S3). Electrochemical surface area (ECSA) of the Au nanofilm was estimated to be 22.0 cm² by calculating the Au reduction peak as compared to a Au wire swept to 1.4 V at a scan rate of 10 mV s⁻¹ and a specific capacitance of 400 μ C cm⁻². When performing the standard addition method in the river water sample the Au reduction peak was compared to that of the ultrapure solution to estimate electrochemical surface area due to an interfering peak at high potentials. When using the Au nanofilm electrode the capacitive current increased but did not obscure the peak due to reduction of the Au surface (Fig. 2B, Peak 2). The capacitance due to the carbon paper is represented by the widening with increasing scan rate observed in the region between 0.45 and 0.8 V.

The Au reduction peak with the Au nanofilm was not statistically different from the Au reduction peak on the Au wire. This could be indicative that the nanofilm is not presenting increased catalytic activity or peak shifting due to nanostructure strain. ⁵⁰ However, a

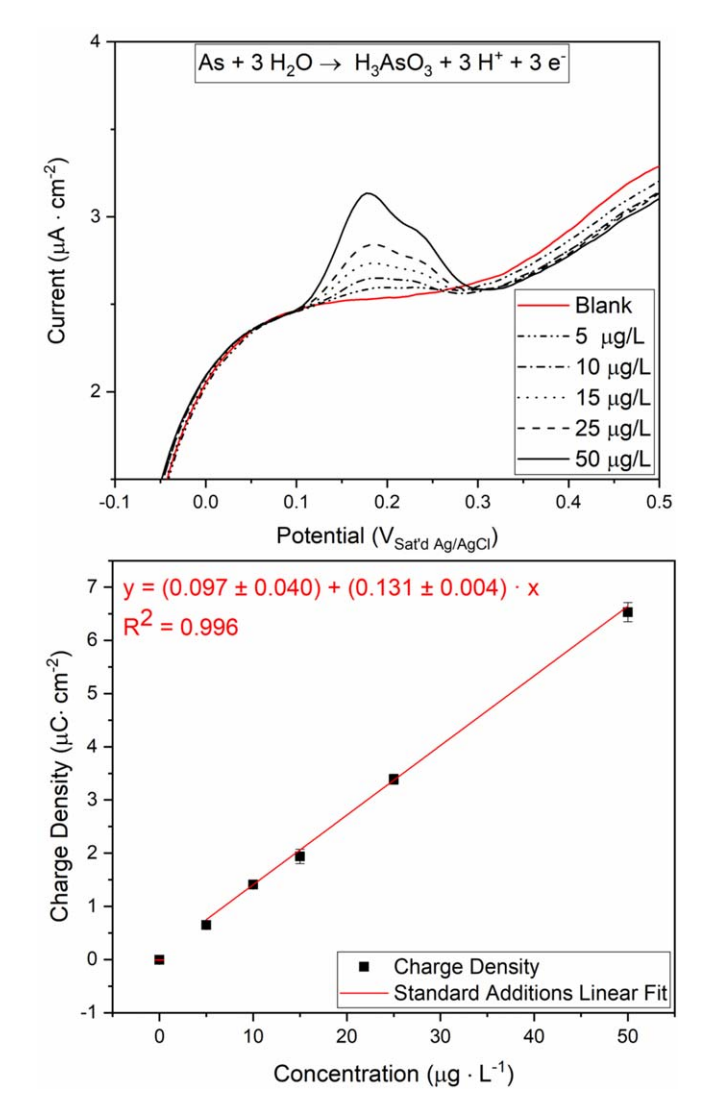


Figure 3. (A) Linear stripping voltammetry results for increasing As (III) concentrations of 5, 10, 25, and 50 $\mu g \cdot l^{-1}$ to ultrapure water with 0.5 M H_2SO_4 supporting electrolyte; (B) linear regression of area under curve between 0.14 and 0.3 V vs As (III) concentration. Average values are shown with error bars representing standard deviation of four replicate stripping processes.

shift in reduction peak maximum potential for the Au nanoparticles could also be caused by resistance due to the high surface area of the XC-72 carbon support.

The Au nanoparticle electrode presented a high capacitive current from XC 72R, which masked faradaic current peaks for Au reduction. Cyclic voltammetry between 0.45 and 1.3 V was performed at 1, 50 and 100 mV s⁻¹. The difference in reduction peak minimum for the Au nanoparticles was statistically significant (p = 0.0002). The nanoparticle electrodes Au reduction potentials were lower than that for the Au wire. This is likely due to the high surface area and surface strain of the Au nanoparticles. Gold nanoparticle electrodes prepared on low surface area carbon supports do not necessarily result in masking of the Au reduction peak from capacitive current. ^{17,23,24,30,51} In our study, the use of Au nanoparticles supported on high surface area carbons, and use of LSV instead of pulse stripping voltammetry, resulted in a large amount of capacitive current and masking of faradaic currents and peaks. Linear stripping voltammetry relies on a high peak to background area for detection of trace As (III), thus the use of XC 72R to create an Au nanoparticle electrode was determined to be unsuitable for

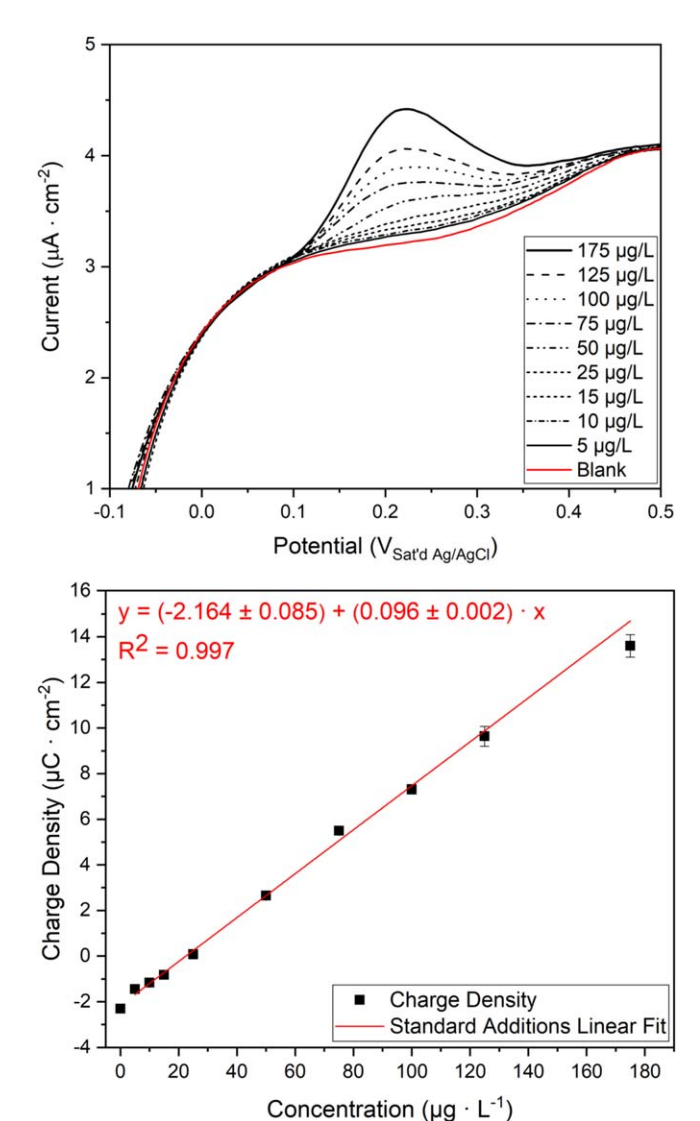


Figure 4. (A) Linear stripping voltammetry results for increasing As (III) concentrations of 5, 10, 15, 20, 25, 50, 75, 100, 125 and 175 $\mu g \cdot l^{-1}$ to Rio Paguate River water sample from Laguna NM, USA, with 0.5 M H₂SO₄; (B) linear regression of area between baseline between 0.1 and 0.4 V and standard additions curves.

As (III) detection. Differential pulse voltammetric methods are capable of greatly decreasing the capacitive background. However, a goal of this study is to minimize the time and complexity of the test procedure and data analysis so that non electrochemist professionals would be capable of performing the analysis without assistance.

The DC sputtering method for generating Au nanofilm electrodes results in a comparatively reduced background, is facile, and is potentially scalable by using already existing large scale manufacturing technologies. In our study DC sputtering benefited from coating a larger amount of carbon support surface area than the chemically deposited nanoparticles, which mitigated masking of faradaic peaks which were observed in the Au nanoparticle cyclic voltammetry. The stability of the DC Sputtered thin films was found to be better than that of the Au nanoparticles because when gas evolution would occur on the electrodes the Au nanoparticles would show a decrease in Au peaks to the point of completely absent. The DC sputtered Au nanofilms could withstand gas evolution without the electrochemical activity of the Au being completely lost. Further study of detection of trace As (III) was conducted only with the Au DC sputtered nanofilm electrodes.

Detection of arsenite in ultrapure conditions with Au nanofilm.—The Au nanofilm showed a statistically significant difference in peak area for oxidation of As (0) to As (III) between standard additions of 5, 10 and 15 μ g l⁻¹ As (III) (Anova p = 1.67E-05, Table SIII) in 18 MΩ DI water acidified with 0.5 M H₂SO₄. Figure 3A shows the linear sweep data for standard additions of 5, 10, 15, 25, and 50 μ g l⁻¹ As (III). The limit of detection was determined to be 0.15 μ g l⁻¹ for the ultrapure calibration curve. The peak area correlated to As oxidation was analyzed by determining the difference between curves and the blank between the beginning and end of the peak. The stripping peak has a shoulder at a slightly more positive potential which can be attributed to a polycrystalline surface with multiple surface energies resulting in multiple peak potentials of stripping. 52,53 The peak was originally thought to be potentially caused by Cu (II) contamination because of the wellknown interference of Cu with the As (III) oxidation during stripping analysis. Careful preparation measures and thorough cleaning procedures were performed to ensure that this was not the case. Figure 3B shows the area under the As (III) peak vs the concentration with error bars representing the standard deviation from analysis of four LSV determinations conducted successively in each concentration during a single standard additions experiment. The plot has an R² value of 0.996 showing a good linear trend between 5, 10, 15, 25, and 50 μ g·l⁻¹, and that the DC sputtered electrode was able to detect As (III) at environmentally and toxicologically important values by creating a calibration curve while using a low loading nanofilm of Au per electrode.

Again, linear stripping was chosen instead of pulse stripping techniques because it does not require individual electrode evaluation. Pulse stripping is effective in reducing background due to capacitive current, but it also requires defining additional parameters such as pulse height, frequency, and pulse width. ^{54,55} In the effort to generate electrodes which can be used for in-field measurements, a reproducible and simple technique for workers which outlines the need for acidification, how to perform standard additions with stock solutions, deposition potentials and time as well as scan rate could make performing electrochemical detection accessible to workers unfamiliar with electrochemistry. ⁵⁶

Detection of arsenite in river water sample with Au nanofilm.— The DC sputtered Au nanofilm electrode was used to detect standard additions of 5, 10, 15, 20, 25, 50, 75, 100, 125 and 175 μ g l⁻¹ As (III) to a river water sample (Fig. 4A). There was not an observed peak from As (III) in the river water sample initially, but there was statistically significant difference in standard additions of 5, 10 and $15 \mu g l^{-1}$ curve area above the baseline (Anova p = 0.00021, Table SIV). The limit of detection was determined to be 4.7 μ g l⁻¹ for the river water sample calibration curve. Metal ion analysis with ICP-MS showed an initial concentration of 5.54 μ g l⁻¹ total As (Table I). The lack of an initial As (III) peak in the acidified sample may be because ICP-MS determined As may have been in the electrochemically inactive As (V) form and therefore undetectable by LSV. This is quite likely considering this was a surface water and the As is more likely to be in a higher oxidation state than in a ground water sample. The peak is broader and does not present the same shape as in the ultrapure water conditions. As can be observed through ICP analysis in Table I there are many commonly occurring ions in the sample which could be contributing to difference in the stripping characteristics of As from the Au nanofilm surface. Broadening could be due to co-adsorption or concentration gradient interferences, however studies which investigate the effects of individual ions present in common natural water matrices on As oxidation shape would be necessary to confirm this and could increase peak sensitivity and selectivity.

The electrode was able to detect at and below the $10~\mu g\,l^{-1}$ MCL in the water sample with the standard addition method. Figure 4B shows the charge density of As oxidation peaks vs As (III) standard additions concentrations ($R^2=0.997$). The linearity of the calibration curve was as good in the water sample as with the ultrapure

water by using the difference in the area under the curve within the peak region and the baseline LSV data. However, the limit of detection was increased from 0.15 to 4.7 μ g l⁻¹. The oxidation of As (III) at lower concentrations resulted in a small but broad increase above the baseline between 0.1 and 0.45 V vs Ag/AgCl. The Au nanofilm could determine at and below the maximum contaminant level with strong linearity using the standard addition method in a source of drinking water for the people of Laguna.

Conclusions

This study shows that DC sputtering deposition of Au nanofilms on conductive substrates is a viable method for generating electrodes for effective As (III) detection with a ultralow loading of Au per electrode and uses current mass manufacturing technologies. The nanofilm showed a strong linear correlation of charge density to As (III) concentration when using the standard additions method in both ultrapure and river water samples. The river water sample was analyzed using ICP MS and OES and IC and contained many common ions found in typical water samples such as alkalinity, nitrates, sulfates, and other metals. These other ions may have contributed to the broadening of the As oxidation peak in comparison to LSV performed in ultrapure conditions. However, further studies into the effects of individual ions on the peak shape would be necessary to come to definitive conclusions. There was not a detectable amount of As (III) in the river water sample, however statistically significant variance between 5, 10, and 15 μ g l⁻¹ (Anova p = 0.00021) and an R^2 value of 0.997 suggest that the As present was likely in the oxidized and electrochemically inactive As (V) valence. The river water sample standard additions peak was broader and showed only one peak where the ultrapure water showed a peak with a shoulder. The two peaks in ultrapure conditions were attributed to the polycrystalline nature of the DC sputtered nanofilm surface, because there was no source of Cu (II) contamination and previous studies show that the crystallographic orientation can present multiple As stripping potentials when using nanostructures.

These results show the electrode is capable of detection below the $10 \ \mu g \ l^{-1}$ MCL in drinking water using LSV. The use of sputter deposition allows for much lower Au loading films, which reduces the cost of Au as compared to screen-printed or wire electrodes. Physical vapor deposition also offers the ability to generate many electrodes at once in a facile and scalable manner. From an electrochemical standpoint DC sputtered films benefit from coating low surface area conductive substrates thus decreasing capacitive current. This was not the case for Au nanoparticles chemically deposited onto the high surface area carbon support of XC 72R which suffered from excessive capacitive current masking.

Forward outlooks for the DC sputtered Au nanofilm electrodes are in preparing a selective and low Au consumption sensor for in-field use coupled with a handheld potentiostat/smartphone. Several studies have incorporated treatment of the samples to chemically reduce electrochemically inactive As (V) to As (III) which could be used to allow this method to determine total As in addition to As (III) in a river water sample. 22,27,57 Additionally, an in-field usability study comparing LSV and differential pulse voltammetry using the DC sputtered Au nanofilm electrodes would allow for determining and quantifying benefits and drawbacks of each method for in situ use. A useability study would include performing the standard additions method in the field and assessing the impacts of deoxygenation. Physical vapor deposition of Au nanofilms offers an alternative method for fabricating low cost As (III) sensing electrodes. The sputtered Au thin film electrodes may also be effective for in field measurement of Cu, Cr, Fe and other ions of interest.

Acknowledgments

This material is based upon work supported by the National Science Foundation Graduate Research Fellowship under grant no. (DGE-1418062), University of New Mexico Center for Water and the Environment, (CREST Grant Number 1345169 and 1914490)

and the Center for Micro-Materials. Any opinion, findings, and conclusions or recommendations expressed in this material are those of the authors(s) and do not necessarily reflect the views of the National Science Foundation.

ORCID

Tybur Q. Casuse https://orcid.org/0000-0003-0685-0084

Angelica Benavidez https://orcid.org/0000-0001-7808-453X

John B. Plumley https://orcid.org/0000-0002-6404-2467

Lok-kun Tsui https://orcid.org/0000-0001-7381-0686

Abdul-Mehdi Ali https://orcid.org/0000-0002-8463-8153

José M. Cerrato https://orcid.org/0000-0002-2473-6376

Fernando H. Garzon https://orcid.org/0000-0002-4511-9932

References

- A. Basu, D. Saha, R. Saha, T. Ghosh, and B. Saha, *Res. Chem. Intermed.*, 40, 447 (2014).
- 2. M. M. Berg, Environ. Sci. Technol., 35, 2621 (2001).
- 3. WHO, (2010), World Health Organization.
- 4. USEPA, (2014), Vol. 40 CFR Part 423, appendix A.
- 5. M. Simmler, *Environ. Pollut.*, **231**, 722 (2017).
- F.-A. Weber, A. F. Hofacker, A. Voegelin, and R. Kretzschmar, *Environ. Sci. Technol.*, 44, 116 (2010).
- 7. C. W. Neil, Environ. Sci. Technol., 48, 4395 (2014).
- 8. Z. Shi, S. Hu, J. Lin, T. Liu, X. Li, and F. Li, *Environ. Sci. Technol.*, **54**, 6621 (2020)
- R. T. Wilkin, R. G. Ford, L. M. Costantino, R. R. Ross, D. G. Beak, and K. G. Scheckel, *Environ. Sci. Technol.*, 53, 11684 (2019).
- 10. D. Renock and J. Voorhis, Environ. Sci. Technol., 51, 3733 (2017).
- 11. D. G. K. P. L. Smedley, Appl. Geochem., 17, 517 (2002).
- 12. D. Q. Hung, O. Nekrassova, and R. G. Compton, *Talanta*, 64, 269 (2004).
- 13. K. D. Reid, F. Goff, and D. A. Counce, N. M. Geol., 25, 75 (2003).
- J. Das Joyati, P. Sarkar, J. Panda, and P. Pal, J. Environ. Sci. Health., A, 49, 108 (2014).
- 15. Metrohm, (2013), (Metrohm, ed.).
- 16. Metrohm, (Metrohm, ed.), Vol. 416. Metrohm, Application Bulletin.
- X. Dai, O. Nekrassova, M. E. Hyde, and R. G. Compton, *Anal. Chem.*, 76, 5924 (2004).
- J. C. Bullen, A. Torres-Huerta, P. Salaun, J. S. Watson, S. Majumdar, R. Vilar, and D. J. Weiss, *Water Res.*, 175, 115650 (2020).
- J. A. Cox, I. A. Rutkowska, and P. J. Kulesza, J. Electrochem. Soc., 167, 037565 (2020).
- 20. M. C. Welch Christine and R. G. Compton, Anal. Bioanal. Chem., 384, 601.
- 21. L. D. Burke and P. F. Nugent, Gold Bull., 30, 43 (1997).
- E. Nunez-Bajo, M. C. Blanco-Lopez, A. Costa-Garcia, and M. T. Fernandez-Abedul, Anal. Chem., 89, 6415 (2017).
- 23. T. Gu et al., *Electrochem. Commun.*, **33**, 43 (2013).

- 24. J.-F. Huang and H.-H. Chen, *Talanta*, 116, 852 (2013).
- 25. B. K. Jena Bikash Kumar and C. R. Raj, Anal. Chem., 80, 4836 (2008).
- X. Dai Xuan, G. G. Wildgoose, C. Salter, A. Crossley, and R. G. Compton, Anal. Chem., 78, 6102 (2006).
- 27. Y. Song and G. M. Swain, Anal. Chim. Acta, 593, 7 (2007).
- E. A. Viltchinskaia, L. L. Ziegman, D. M. Garcia, and P. F. Santos, *Electroanalysis*, 9, 633 (1996).
- J. Wu, M. Yang, J. Xiao, X. Fu, J. Jin, L. Li, W. Chang, and C. Xie, *J. Electrochem. Soc.*, 160, B225 (2013).
- 30. D. Kato, T. Kamata, D. Kato, H. Yanagisawa, and O. Niwa, *Anal. Chem.*, **88**, 2944
- 31. S. A. Kumar, S.-F. Wang, and Y.-T. Chang, *Thin Solid Films*, 518, 5832 (2010).
- Q. M. Mehran, M. A. Fazal, A. R. Bushroa, and S. Rubaiee, Crit. Rev. Solid State Mater. Sci., 43, 158 (2017).
- S. Shahidi, B. Moazzenchi, and M. Ghoranneviss, Eur. Phys. J. Appl. Phys., 71, 31302 (2015).
- M. Kim, W.-J. Ha, J.-W. Anh, H.-S. Kim, S.-W. Park, and D. Lee, *J. Alloys Compd.*, 484, 28 (2009).
- A. K. Mo, V. L. Brown, B. K. Rugg, T. C. DeVore, H. M. Meyer, X. Hu, W. C. Hughes, and B. H. Augustine, *Adv. Funct. Mater.*, 23, 1431 (2013).
- S. Tanami, D. Ichida, S. Hashimoto, H. Seo, D. Yamashita, N. Itagaki, K. Koga, and M. Shiratani, *Thin Solid Films*, 641, 59 (2017).
- 37. K. Kim, J. Park, H. Kim, G. Y. Jung, and M.-G. Kim, *ACS Catal.*, **9**, 9206 (2019).
- J. van der Zalm, S. Chen, W. Huang, and A. Chen, J. Electrochem. Soc., 167, 037532 (2020).
- 39. J. Jiang and C. Wang, J. Electrochem. Soc., 167, 037521 (2020).
- J. Thangphatthanarungruang, A. Lomae, O. Chailapakul, S. Chaiyo, and W. Siangproh, *Electroanalysis*, 33, 226 (2020).
- A. Pringkasemchai, F. Hoshyargar, B. Lertanantawong, and A. P. O'Mullane, *Electroanalysis*, 31, 2095 (2019).
- N. R. Devi, M. Sasidharan, and A. K. Sundramoorthy, J. Electrochem. Soc., 165, B3046 (2018).
- 43. M. Carmo, M. Linardi, and J. G. R. Poco, Appl. Catal. A Gen., 355, 132 (2009).
- 44. L. Prati and G. Martra, Gold Bull., 32, 96 (1999).
- 45. J. M. Blake et al., *Environ. Sci. Process Impacts*, 19, 605 (2017).
- L. M. Fischer, M. Tenje, A. R. Heiskanen, N. Masuda, J. Castillo, A. Bentien, J. Émneus, M. H. Jakobsen, and A. Boisen, *Microelectron. Eng.*, 86, 1282 (2009).
- 47. S. Palli and S. R. Dey, Adv. Mater. Sci., 2, 1 (2017).
- 48. C. V. Thompson, Annu. Rev. Mater. Sci., 30, 159 (2000).
- 49. P. Wei, F. Katmis, C. Z. Chang, and J. S. Moodera, Nano Lett., 16, 2714 (2016).
- 50. X. Luo, A. Morrin, A. J. Killard, and M. R. Smyth, Electroanalysis, 18, 319 (2006).
- D.-D. Han, S.-S. Li, Z. Guo, X. Chen, J.-H. Liu, and X.-J. Huang, RSC Adv., 6, 30337 (2016).
- J. M. Feliu, A. Fernandez-Vega, A. Aldaz, and J. Clavilier, J. Electroanal. Chem. Interfacial Electrochem., 256, 149 (1988).
- B. Ren, L. A. Jones, M. Chen, D. K. Oppedisano, D. Qiu, S. J. Ippolito, and S. K. Bhargava, J. Electrochem. Soc., 164, H1121 (2017).
- G. Forsberg, J. W. Olaughlin, R. G. Megargle, and S. R. Koirtyohann, *Anal. Chem.*, 47, 1586 (1975).
- 55. T. K. Copeland, Anal. Chem., 45, 2171 (1973).
- 56. R. T. Kachoosangi and R. G. Compton, Sens. Actuators B Chem., 178, 555 (2013).
- 57. F. T. Henry, *Anal. Chem.*, **51**, 215 (1979).